Varying the chiral magnetic effect relative to flow in a single nucleus-nucleus collision *

Hao-Jie Xu(徐浩洁)[1] Jie Zhao(赵杰)[2] Xiao-Bao Wang(王小保)[1] Han-Lin Li(李汉林)[3]
Zi-Wei Lin(林子威)[4,5] Cai-Wan Shen(沈彩万)[1] Fu-Qiang Wang(王福强)[1,2;1)]

[1] School of Science, Huzhou University, Huzhou, Zhejiang 313000, China
[2] Department of Physics and Astronomy, Purdue University, West Lafayette, Indiana 47907, USA
[3] College of Science, Wuhan University of Science and Technology, Wuhan, Hubei 430065, China
[4] Department of Physics, East Carolina University, Greenville, North Carolina 27858, USA
[5] Key Laboratory of Quarks and Lepton Physics (MOE) and Institute of Particle Physics, Central China Normal University, Wuhan, Hubei 430079, China

Abstract: We propose a novel method to search for the chiral magnetic effect (CME) in heavy ion collisions. We argue that the relative strength of the magnetic field (mainly from spectator protons and responsible for the CME) with respect to the reaction plane and the participant plane is opposite to that of the elliptic flow background arising from the fluctuating participant geometry. This opposite behavior in a single collision system, hence with small systematic uncertainties, can be exploited to extract the possible CME signal from the flow background. The method is applied to existing data from RHIC, and the outcome discussed.

Keywords: heavy ion collision, chiral magnetic effect, charge separation, reaction plane, participant plane, event plane

PACS: 25.75.-q, 25.75.Gz, 25.75.Ld **DOI:** 10.1088/1674-1137/42/8/084103

1 Introduction

One of the fundamental properties of quantum chromodynamics (QCD) is the creation of topological gluon fields from vacuum fluctuations in local domains [1–3]. Interactions with those gluon fields can change the handedness (chirality) of quarks, under restoration of the approximate chiral (χ) symmetry, which can lead to local parity and charge-conjugate parity violations [3–5]. These violations in the early universe could be responsible for the matter-antimatter asymmetry [6] and are of fundamental importance. The resulting chirality imbalance, often referred to as the topological charge (Q_w), can lead to an electric current, or charge separation (CS), along a strong magnetic field (B), a phenomenon called the chiral magnetic effect (CME) [7]. Such phenomena are not specific to QCD but are a subject of interest to a wide range of physics communities [8], e.g. condensed matter and material physics [9–11].

Both conditions for the CME– the χ-symmetry and a strong B [8] – may be met in relativistic heavy ion collisions (HIC), where a high energy-density state of deconfined quarks and gluons (the quark-gluon plasma) is formed, resembling the conditions of the early universe [12–16]. At high energies, a nucleus-nucleus collision can be considered as being composed of participant nucleons in an overlap interaction zone, with the remaining spectator nucleons passing by and continuing into the beam line (see the sketch of a nucleus-nucleus collision in Fig. 1). The spectator protons produce the majority of B, whose direction is, on average, perpendicular to the reaction plane (RP) spanned by the impact parameter (b) and beam directions. The sign of Q_w is, however, random, due to its fluctuating nature; consequently the CS dipole direction is random [5]. As a result the CS can only be measured by charge correlations. A commonly used observable is the three-point azimuthal correlator [17], $\gamma \equiv \langle \cos(\phi_\alpha + \phi_\beta - 2\psi_{\rm RP}) \rangle$, where ϕ_α and ϕ_β are the azimuths of two charged particles, and $\psi_{\rm RP}$ is that of the RP. Because of charge-independent backgrounds, such as correlations from global momentum conservation, the correlator difference between opposite-sign (OS) and same-sign (SS) pairs, $\Delta\gamma \equiv \gamma_{\rm OS} - \gamma_{\rm SS}$, is used. However, $\Delta\gamma$ is ambiguous between a back-to-back pair perpendicular to the RP (potential CME signal) and an aligned pair in the RP (e.g. from resonance decay). There are generally more

Received 26 April 2018, Published online 13 July 2018
* Supported by National Natural Science Foundation of China (11647306, 11747312, U1732138, 11505056, 11605054, 11628508) and US Department of Energy (DE-SC0012910)
1) E-mail: fqwang@zjhu.edu.cn
©2018 Chinese Physical Society and the Institute of High Energy Physics of the Chinese Academy of Sciences and the Institute of Modern Physics of the Chinese Academy of Sciences and IOP Publishing Ltd

particles (including resonances) produced along the RP than perpendicular to it, the magnitude of which is characterized by the elliptic anisotropy parameter (v_2) [18]. It is commonly interpreted as coming from a stronger hydrodynamic push in the short-axis (i.e. RP) direction of the elliptically-shaped overlap zone between the two colliding nuclei [19]. As a result, $\Delta\gamma$ is contaminated by a background [17, 20–24], which arises from the coupling between particle correlations and v_2, and is hence proportional to v_2.

The search for the CME is one of the most active research topics in HIC at the Relativistic Heavy Ion Collider (RHIC) and the Large Hadron Collider (LHC) [25–33]. A finite $\Delta\gamma$ signal is observed [25–29], but how much background contamination there is has not yet been settled. There have been many attempts to gauge, reduce or eliminate the flow backgrounds, by event-by-event v_2 dependence [30], event-shape engineering [32, 33], comparisons with small-system collisions [31, 32, 34], invariant mass studies [35], and by new observables [36, 37]. The LHC data seem to suggest that the CME signal is small and consistent with zero [32, 33], while the situation at RHIC is less clear [8].

To better gauge background contributions, isobaric ${}^{96}_{44}$Ru+${}^{96}_{44}$Ru (RuRu) and ${}^{96}_{40}$Zr+${}^{96}_{40}$Zr (ZrZr) collisions have been proposed [38] and are planned for RHIC in 2018. Their QCD backgrounds are expected to be almost the same because of the same mass number, whereas the atomic numbers, hence B, differ by 10%. These expectations are qualitatively confirmed by studies [39] with Woods-Saxon (WS) nuclear densities; the CME signal over background could be improved by a factor of seven in relative measurements of RuRu and ZrZr collisions compared to either of them individually. In a recent study [40], however, we have shown that there could exist large uncertainties in the differences in both the overlap geometry eccentricity (ϵ_2) and B due to nuclear density deviations from WS. As a result, isobaric collisions may not provide a clear-cut answer to the existence or the lack of the CME.

In what follows, we argue that one has, in a single collision system, all the advantages of, to an even better degree, the significant B and minimal ϵ_2 differences of the comparative isobaric collisions, with the benefit of minimal theoretical and experimental uncertainties. The idea is straightforward, as illustrated in Fig. 1. B is produced by spectator protons, hence its projection, on average, is strongest perpendicular to the RP [5]; v_2 stems from the collision geometry and is strongest with respect to the second harmonic participant plane (PP) [41]. The RP and the PP are correlated but, due to fluctuations [41], not identical. Measurements with respect to the RP and the PP, therefore, contain different amounts of CME signal and v_2 background, and thus can help disentangle the two contributions.

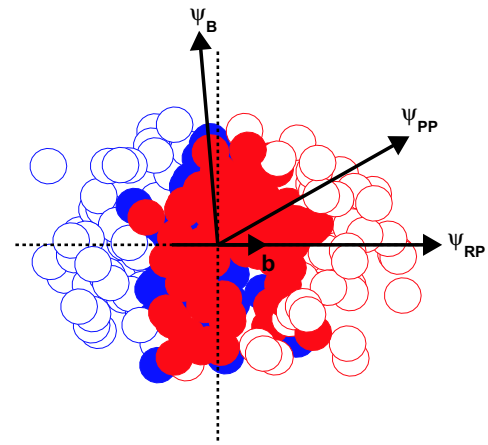

Fig. 1. (color online) Sketch of a heavy ion collision projected onto the transverse plane (perpendicular to the beam direction). $\psi_{\rm RP}$ is the reaction plane (impact parameter, b) direction, $\psi_{\rm PP}$ the participant plane direction (of interacting nucleons, denoted by the solid circles), and $\psi_{\rm B}$ the magnetic field direction (mainly from spectator protons, denoted by the open circles together with spectator neutrons).

2 General idea

Due to fluctuations, the PP azimuthal angle ($\psi_{\rm PP}$) is not necessarily aligned with the RP azimuthal angle [41]. The v_2 is directly related to the eccentricity of the transverse overlap geometry, $\epsilon_2\{\psi_{\rm PP}\}\equiv\langle\epsilon_2\{\psi_{\rm PP}\}_{\rm evt}\rangle$. The average is taken over the event-by-event eccentricity magnitudes, which can be obtained by [40–44]

$$\epsilon_2\{\psi_{\rm PP}\}_{\rm evt}{\rm e}^{{\rm i}2\psi_{\rm PP}}=\sum_{i=1}^{N_{\rm part}}\left(r_{\perp i}^2{\rm e}^{{\rm i}2\phi_{r\perp i}}\right)\Bigg/\sum_{i=1}^{N_{\rm part}}r_{\perp i}^2\,, \qquad (1)$$

where $(r_{\perp i},\phi_{r\perp i})$ is the polar coordinate of the i-th participant nucleon. The overlap geometry relative to b, averaged over many events, is an ellipse with its short axis along the RP; its eccentricity is

$$\epsilon_2\{\psi_{\rm RP}\}=\langle\epsilon_2\{\psi_{\rm PP}\}_{\rm evt}\cos2(\psi_{\rm PP}-\psi_{\rm RP})\rangle. \qquad (2)$$

Let

$$a^{\rm PP}\equiv\langle\cos2(\psi_{\rm PP}-\psi_{\rm RP})\rangle \qquad (3)$$

measure the correlation between $\psi_{\rm PP}$ and $\psi_{\rm RP}$. We have

$$a^{\rm PP}_{\epsilon_2}\equiv\epsilon_2\{\psi_{\rm RP}\}/\epsilon_2\{\psi_{\rm PP}\}\approx a^{\rm PP}. \qquad (4)$$

The factorization is approximate, valid only when, at a given collision centrality, the $\epsilon_2\{\psi_{\rm PP}\}_{\rm evt}$ magnitude does not vary with the $\psi_{\rm PP}$ fluctuation around $\psi_{\rm RP}$.

B is mainly produced by spectator protons. Their positions fluctuate; the B azimuthal direction, $\psi_{\rm B}$, is not always perpendicular to the RP [45–47] (see illustration in Fig. 1). The CME-induced CS is along the B direction

[5]; when measured perpendicular to a direction ψ, its relevant strength is proportional to $B_{\rm sq}\{\psi\} \equiv \langle (eB(\mathbf{0},0)/m_\pi^2)^2\cos 2(\psi_{\rm B}-\psi)\rangle$ [39]. Although the field point $\boldsymbol{r}=0$ is used here, other field points are also calculated and our conclusion does not change. The overall magnetic field strength is calculated at $t=0$. In general, the magnetic field changes when the system evolves, and there are large theoretical uncertainties. However, as we will show that only the relative difference is used in our method, the absolute magnitudes of the magnetic field do not affect our conclusions. Because the position fluctuations of participant nucleons and spectator protons are independent except for the overall constraint of the nucleus, $\psi_{\rm PP}$ and $\psi_{\rm B}$ fluctuate independently about $\psi_{\rm RP}$. This yields

$$a^{\rm PP}_{B_{\rm sq}} \equiv B_{\rm sq}\{\psi_{\rm PP}\}/B_{\rm sq}\{\psi_{\rm RP}\} \approx a^{\rm PP}. \tag{5}$$

Because B also contains contributions from participant protons, the factorization is only approximate. We calculate $B(\boldsymbol{r},t)$ by [45–47]

$$eB(\boldsymbol{r},t)=\sum_i \alpha_{\rm EM} Z_i(\boldsymbol{r}'_i)\frac{1-v_i^2}{[r_i'^2-(\boldsymbol{r}'_i\times\boldsymbol{v}_i)^2]^{3/2}}\boldsymbol{v}_i\times\boldsymbol{r}'_i, \tag{6}$$

where $\boldsymbol{v}_i$ is the velocity of the i-th proton, $\boldsymbol{r}'_i=\boldsymbol{r}-\boldsymbol{r}_i(t)$ is the relative distance between the field point $\boldsymbol{r}$ and the proton position $\boldsymbol{r}_i(t)$ at time t, $\alpha_{\rm EM}=1/137$, and $Z_i(\boldsymbol{r}'_i)$ is the charge number factor. After employing a finite proton radius $r_{\rm p}=0.88$ fm, $Z_i(\boldsymbol{r}'_i)=1$ if $\boldsymbol{r}$ is located outside the proton and $Z_i(\boldsymbol{r}'_i)<1$ depends on $\boldsymbol{r}'_i$ if $\boldsymbol{r}$ is located inside the proton [47]. Varying the $r_{\rm p}$ value has little effect on our results.

It is convenient to define a relative difference [39],

$$R^{\rm PP(EP)}(X)\equiv 2\cdot\frac{X\{\psi_{\rm RP}\}-X\{\psi_{\rm PP(EP)}\}}{X\{\psi_{\rm RP}\}+X\{\psi_{\rm PP(EP)}\}}, \tag{7}$$

where $X\{\psi_{\rm RP}\}$ and $X\{\psi_{\rm PP(EP)}\}$ are the measurements of quantity X with respect to $\psi_{\rm RP}$ and $\psi_{\rm PP}$ (or $\psi_{\rm EP}$ described below), respectively. Those in ϵ_2 and $B_{\rm sq}$ are

$$\begin{aligned} R^{\rm PP}(\epsilon_2) &\equiv -2(1-a^{\rm PP}_{\epsilon_2})/(1+a^{\rm PP}_{\epsilon_2}) \approx -R_{\rm PP}, \\ R^{\rm PP}(B_{\rm sq}) &\equiv 2(1-a^{\rm PP}_{B_{\rm sq}})/(1+a^{\rm PP}_{B_{\rm sq}}) \approx R_{\rm PP}, \end{aligned} \tag{8}$$

where

$$R_{\rm PP}\equiv 2(1-a^{\rm PP})/(1+a^{\rm PP}). \tag{9}$$

The upper panels of Fig. 2 show $R^{\rm PP}(\epsilon_2)$ and $R^{\rm PP}(B_{\rm sq})$ calculated by a Monte Carlo Glauber model (MCG) [42–44, 48] for ${}^{197}_{79}$Au+${}^{197}_{79}$Au (AuAu), ${}^{62}_{29}$Cu+${}^{62}_{29}$Cu (CuCu), RuRu, ZrZr collisions at RHIC and ${}^{207}_{82}$Pb+${}^{207}_{82}$Pb (PbPb) collisions at the LHC. The centrality percentage is determined from the impact parameter, $b=|\boldsymbol{b}|$, in MCG. For a given b drawn from the probability distribution $P(b)\propto b$, a participant nucleon is determined by its relative transverse distance d from the surrounding nucleons in the other nucleus, according to the nucleon-nucleon differential cross section $d^2\sigma_{\rm NN}/d^2d=A\exp(-\pi A d^2/\sigma_{\rm NN})$ [49]. We use $A=0.92$; $\sigma_{\rm NN}=42$ mb for AuAu, CuCu, RuRu and ZrZr collisions and $\sigma_{\rm NN}=62.4$ mb for PbPb collisions. The minimum inter-nucleon distance in each nucleus is set to be $d_{\rm min}=0.4$ fm. Varying $\sigma_{\rm NN}$ and $d_{\rm min}$ does not change our results significantly. At the same energy (RHIC), the smaller the system, the larger the fluctuations and hence the larger the $R^{\rm PP}(\epsilon_2)$ and $R^{\rm PP}(B_{\rm sq})$ magnitudes. The larger LHC value for PbPb than the RHIC value for AuAu is due to the larger nucleon-nucleon cross section ($\sigma_{\rm NN}$) used at LHC than at RHIC.

Spherical nuclei with the WS as well as the energy density functional theory (DFT) [50, 51] calculated distributions [40] are used. The uncertainties in the DFT calculations, assessed by using different mean fields (SLy4 and SLy5 [52], and SkM* [53]), with (Hartree-Fock-Bogoliubov) and without (Hartree-Fock) pairing correlations [50, 54, 55], and varying the nuclear deformations [40], are all small in our results. The results are compared to the corresponding $\pm R_{\rm PP}$: the approximations in Eqs. (4) and (5) are good. The PP is not experimentally measured, nor is ϵ_2. As a proxy for PP, the event plane (EP) is often reconstructed by $v_2\{\psi_{\rm EP}\}_{\rm evt}{\rm e}^{{\rm i}2\psi_{\rm EP}}=\langle {\rm e}^{i2\phi}\rangle$, similar to Eq. (1), but using the final-state charged particle azimuthal angle ϕ in momentum space [56].

The v_2 is measured by the EP method with a correction for the EP resolution ($\mathcal{R}_{\rm EP}$), $v_2\{\psi_{\rm EP}\}=\langle\cos 2(\phi-\psi_{\rm EP})\rangle/\mathcal{R}_{\rm EP}$, where ϕ is the particle momentum azimuthal angle, or almost equivalently, by two-particle correlations, $v_2\{\psi_{\rm EP}\}\approx v_2\{2\}\equiv\langle\cos 2(\phi_\alpha-\phi_\beta)\rangle^{1/2}$ [56]. The EP resolution $\mathcal{R}_{\rm EP}$ is calculated by the subevent method with an iterative procedure, dividing the particles randomly into two subevents [56]. A v_2 can also be obtained with respect to the RP, $v_2\{\psi_{\rm RP}\}\equiv\langle\cos 2(\phi-\psi_{\rm RP})\rangle$. Although a theoretical concept, the RP may be assessed by zero-degree calorimeters (ZDC) measuring sidewards-kicked spectator neutrons (directed flow v_1) [18, 57, 58]. Similar to Eqs. (3,4), let

$$a^{\rm EP}=\langle\cos 2(\psi_{\rm EP}-\psi_{\rm RP})\rangle/\mathcal{R}_{\rm EP}, \tag{10}$$

and we have

$$a^{\rm EP}_{v_2}\equiv v_2\{\psi_{\rm RP}\}/v_2\{\psi_{\rm EP}\}\approx a^{\rm EP}. \tag{11}$$

As $B_{\rm sq}\{\psi_{\rm PP}\}$, one can obtain $B_{\rm sq}\{\psi_{\rm EP}\}=\langle(eB(\mathbf{0},0)/m_\pi^2)^2\cos 2(\psi_{\rm B}-\psi_{\rm EP})\rangle/\mathcal{R}_{\rm EP}$, and a similar relationship to Eq. (5),

$$a^{\rm EP}_{B_{\rm sq}}\equiv B_{\rm sq}\{\psi_{\rm EP}\}/B_{\rm sq}\{\psi_{\rm RP}\}\approx a^{\rm EP}. \tag{12}$$

The relative differences in v_2 and $B_{\rm sq}$ are

$$\begin{aligned} R^{\rm EP}(v_2) &\equiv -2(1-a^{\rm EP}_{v_2})/(a^{\rm EP}_{v_2}+1) \approx -R_{\rm EP}, \\ R^{\rm EP}(B_{\rm sq}) &\equiv 2(1-a^{\rm EP}_{B_{\rm sq}})/(1+a^{\rm EP}_{B_{\rm sq}}) \approx R_{\rm EP}, \end{aligned} \tag{13}$$

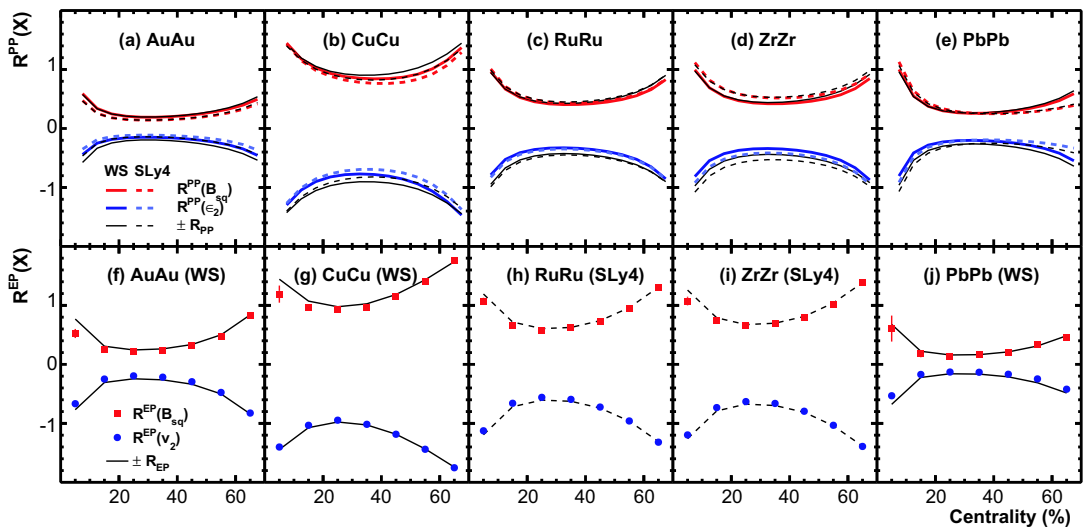

Fig. 2. (color online) Relative differences $R^{\rm PP}(\epsilon_2)$, $R^{\rm PP}(B_{\rm sq})$, $R^{\rm PP}$ from MCG (upper panel) and $R^{\rm EP}(v_2)$, $R^{\rm EP}(B_{\rm sq})$, $R^{\rm EP}$ from AMPT (lower panel) for (a,f) AuAu, (b,g) CuCu, (c,h) RuRu, and (d,i) ZrZr at RHIC, and (e,j) PbPb at the LHC. Both the WS and DFT-calculated densities are shown for the MCG results, while the density profiles used are noted for the AMPT results. Errors, mostly smaller than the symbol size, are statistical.

where

$$R_{\rm EP}\equiv 2(1-a^{\rm EP})/(1+a^{\rm EP}). \tag{14}$$

The lower panels of Fig. 2 show A Multi-Phase Transport (AMPT, "string melting") simulation results of $R^{\rm EP}(v_2)$ and $R^{\rm EP}(B_{\rm sq})$, compared to $\pm R_{\rm EP}$. Again, good agreement is found. The AMPT centrality is determined from the midrapidity ($|\eta|<1$) final-state charged particle multiplicity [40], similar to experiments [59]. Details of AMPT can be found in Refs. [60–63]. The AMPT version (v2.26t5) and parameter values used in the present work are the same as those used earlier for RHIC collisions in Refs. [35, 62, 64–67]; the same parameter setting is used for LHC energy. The MCG and AMPT results cannot be readily compared quantitatively because the former involves PP while the latter uses EP as it would be in experiments. Although AMPT employs MCG as its initial geometry, the subsequent parton-parton scatterings in AMPT are important for the final-state EP determination. In addition, other distinctions exist, such as the nuclear shadowing effect and the Gaussian implementation of $\sigma_{\rm NN}$, which yield different predictions for the eccentricity (hence flow harmonics) and its fluctuations [44, 68]. Nevertheless, the general features are similar between the MCG and AMPT results. Both show opposite behavior for $R^{\rm PP(EP)}(\epsilon_2(v_2))$ and $R^{\rm PP(EP)}(B_{\rm sq})$, which are approximately equal to $\pm R_{\rm PP(EP)}$.

The commonly used $\Delta\gamma$ variable contains, in addition to the CME it is designed for, v_2-induced background,

$$\Delta\gamma\{\psi\}={\rm CME}(B_{\rm sq}\{\psi\})+{\rm BKG}(v_2\{\psi\}). \tag{15}$$

$\Delta\gamma\{\psi\}$ can be measured with respect to $\psi=\psi_{\rm RP}$ (using the 1st order event plane ψ_1 by the ZDC) and $\psi=\psi_{\rm EP}$ (2nd order event plane ψ_2 via final-state particles). If ${\rm BKG}(v_2)$ is proportional to v_2 [17, 20–24] and ${\rm CME}(B_{\rm sq})$ to $B_{\rm sq}$ [47], then

$$R^{\rm EP}(\Delta\gamma)=2\frac{r(1-a^{\rm EP}_{B_{\rm sq}})-(1-a^{\rm EP}_{v_2})}{r(1+a^{\rm EP}_{B_{\rm sq}})+(1+a^{\rm EP}_{v_2})}\approx\frac{1-r}{1+r}R^{\rm EP}(v_2). \tag{16}$$

Here $r\equiv{\rm CME}(B_{\rm sq}\{\psi_{\rm RP}\})/{\rm BKG}(v_2\{\psi_{\rm EP}\})$ can be considered as the relative CME signal to background contribution,

$$r=\frac{1+a^{\rm EP}_{v_2}}{1+a^{\rm EP}_{B_{\rm sq}}}\frac{R^{\rm EP}(\Delta\gamma)-R^{\rm EP}(v_2)}{R^{\rm EP}(B_{\rm sq})-R^{\rm EP}(\Delta\gamma)}\approx\frac{R^{\rm EP}(v_2)-R^{\rm EP}(\Delta\gamma)}{R^{\rm EP}(v_2)+R^{\rm EP}(\Delta\gamma)}. \tag{17}$$

If the experimental measurement $R^{\rm EP}(\Delta\gamma)$ equals $R^{\rm EP}(v_2)$ (i.e. $\Delta\gamma$ scales like v_2), then the CME contribution is zero; if $R^{\rm EP}(\Delta\gamma)\approx -R^{\rm EP}(v_2)$ (i.e. $\Delta\gamma$ scales like $B_{\rm sq}$), then the background is close to zero and all would be CME; and if $R(\Delta\gamma)=0$, then background and CME contributions are of similar magnitudes. The CME signal fractions with respect to RP and EP are, respectively,

$$\begin{aligned} f^{\rm RP}_{\rm CME} &= {\rm CME}(B_{\rm sq}\{\psi_{\rm RP}\})/\Delta\gamma\{\psi_{\rm RP}\}=r/(r+a^{\rm EP}_{v_2}),\\ f^{\rm EP}_{\rm CME} &= {\rm CME}(B_{\rm sq}\{\psi_{\rm EP}\})/\Delta\gamma\{\psi_{\rm EP}\}=r/(r+1/a^{\rm EP}_{B_{\rm sq}}). \end{aligned} \tag{18}$$

3 Application to data

The quantities $a^{\rm PP}$ and $a^{\rm EP}$, and consequently $R^{\rm PP}$ and $R^{\rm EP}$, are mainly determined by fluctuations. Being defined in a single nucleus-nucleus collision, they are insensitive to many details, such as the structure functions of the colliding nuclei. This is in contrast to comparisons

between two isobaric collision systems where large theoretical uncertainties are present [40]. There has been tremendous progress over the past decade in our understanding of the nuclear collision geometry and fluctuations [69]. The MCG and AMPT calculations of these quantities are therefore on rather firm ground.

Table 1. STAR midrapidity ($|\eta|<1$) charged particle v_2 (in percent) in 200A GeV AuAu collisions as functions of centrality (number of participants $N_{\rm part}$ from Ref. [59]): $v_2^{\rm ZDC}$ [70], $v_2^{\rm FTPC}$ [71], and $R^{\rm exp}(v_2)\equiv 2(v_2^{\rm ZDC}-v_2^{\rm FTPC})/(v_2^{\rm ZDC}+v_2^{\rm FTPC})$ compared to $R^{\rm PP}(\epsilon_2)$ from MCG and $R^{\rm EP}(v_2)$ from AMPT. Also listed are $v_2^{\rm TPC}$, $v_2\{2\}$, and $v_2\{4\}$ [72], followed by the three-point correlator $\Delta\gamma\{\psi_2\}$ and $\Delta\gamma\{\psi_1\}$ measurements [25, 26, 28].

cent.(%)	$N_{\rm part}$	$v_2^{\rm ZDC}$	$v_2^{\rm FTPC}$	$R^{\rm exp}(v_2)$	$R^{\rm PP}(\epsilon_2)$	$R^{\rm EP}(v_2)$	$v_2^{\rm TPC}$	$v_2\{2\}$	$v_2\{4\}$	$\Delta\gamma\{\psi_2\}\times10^4$	$\Delta\gamma\{\psi_1\}\times10^4$
50–60	49.3	5.90	7.15	−0.19	−0.240	−0.478	7.30	7.59	6.18	5.133±0.061	5.07±1.60
40–50	78.3	6.40	7.34	−0.14	−0.176	−0.285	7.25	7.64	6.43	3.393±0.026	3.99±0.77
30–40	117.1	6.25	7.00	−0.11	−0.145	−0.219	6.92	7.29	6.33	2.248±0.012	2.18±0.44
20–30	167.6	5.70	6.17	−0.08	−0.147	−0.197	6.09	6.42	5.66	1.424±0.007	1.56±0.31
20–60		5.94	6.59	−0.10	−0.155	−0.227	6.52	6.86	5.96	2.067±0.007	2.19±0.24

Experimentally, $R^{\rm EP}(v_2)$ can be assessed by v_2 measurements. $R^{\rm EP}(B_{\rm sq})$ cannot but may be approximated by $-R^{\rm EP}(v_2)$, as demonstrated by the MCG and AMPT calculations. Table 1 shows the measured v_2 in 200A GeV AuAu collisions by STAR via the ZDC ψ_1 at beam rapidities ($v_2^{\rm ZDC}$) [70] and the forward time projection chamber (FTPC) ψ_2 (i.e. $\psi_{\rm EP}$) at forward/backward rapidities ($v_2^{\rm FTPC}$) [71], together with those via the midrapidity TPC EP ($v_2^{\rm TPC}$) and the two- and four-particle cumulants ($v_2\{2\}$, $v_2\{4\}$) [72]. The relative difference ($R^{\rm exp}(v_2)$) between $v_2^{\rm ZDC}$ and $v_2^{\rm FTPC}$ is smaller in magnitude than $R^{\rm PP}(\epsilon_2)$ from MCG and $R^{\rm EP}(v_2)$ from AMPT; moreover, $v_2^{\rm FTPC}$ may already be on the too-large side as it is larger than $v_2^{\rm TPC}$ for some of the centralities, whereas the opposite is expected because of a smaller nonflow contribution to $v_2^{\rm FTPC}$ [69, 73]. These may suggest that $v_2^{\rm ZDC}$ may not measure the v_2 purely relative to the RP, but a mixture of RP and PP. This is possible because, for instance, the ZDC could intercept not only spectator neutrons but also those having suffered only small-angle elastic scatterings.

Table 1 also lists the $\Delta\gamma$ correlator measurements by STAR with respect to ψ_2 [25, 26, 28] and ψ_1 [28]. Although ψ_1 from ZDC may not strictly measure the RP, our general formulism is still valid, and one can in principle extract the CME signal from those $\Delta\gamma$ measurements. Many of the experimental systematics related to event and track quality cuts cancel in their relative difference $R^{\rm exp}(\Delta\gamma)\equiv 2(\Delta\gamma\{\psi_1\}-\Delta\gamma\{\psi_2\})/(\Delta\gamma\{\psi_1\}-\Delta\gamma\{\psi_2\})$. The remaining major systematic uncertainty comes from the determinations of the RP and EP resolutions or the v_2 [25, 26]. In the STAR $\Delta\gamma\{\psi_2\}$ measurement [25, 26], $v_2^{\rm FTPC}$ [71] was used and the systematic uncertainty was taken to be half the difference between $v_2\{2\}$ and $v_2\{4\}$. In the later STAR measurement [28], the $\Delta\gamma\{\psi_2\}$ uncertainty is taken to be the difference between $\Delta\gamma\{\psi_2\}$ and $\Delta\gamma\{\psi_1\}$, perceived to be physically equal, but shown not to be the case by the present work. Below we use the latter, higher statistics data [28] but the earlier systematic uncertainty estimation [25, 26]. The systematic uncertainty was not estimated for $\Delta\gamma\{\psi_1\}$ [28], though statistical uncertainties are large and likely dominate. We average the v_2 and $\Delta\gamma$ measurements over the centrality range 20%–60%, weighted by $N_{\rm part}^2$ (because the $\Delta\gamma$ is a pair-wise average quantity). We extract the CME to BKG ratio by Eq. (17), replacing $R^{\rm EP}$ with $R^{\rm exp}$ and assuming $a_{B_{\rm sq}}^{\rm EP}=a_{v_2}^{\rm EP}$, so $R^{\rm exp}(B_{\rm sq})=-R^{\rm exp}(v_2)$. We vary the "true" v_2 over the wide range between $v_2\{2\}$ and $v_2\{4\}$, and at each v_2 the $\Delta\gamma\{\psi_2\}$ is replaced by $\Delta\gamma\{\psi_2\}v_2^{\rm FTPC}/v_2$ (i.e. the three-particle correlator measurement divided

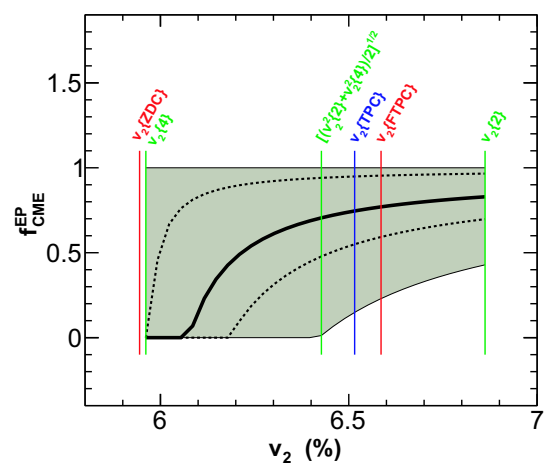

Fig. 3. (color online) Fraction of CME contribution in the $\Delta\gamma\{\psi_2\}$ measurement [25, 26, 28] in the 20%–60% centrality range in 200A GeV AuAu collisions at RHIC versus "true" v_2. The gray area indicates the $\pm1\sigma$ statistical uncertainty, dominated by that in $\Delta\gamma\{\psi_1\}$ [28]. The dashed curves would be the new $\pm1\sigma$ uncertainty with a ten-fold increase in statistics.

by v_2). The fraction $f_{\rm CME}^{\rm EP}$ is obtained and shown in Fig. 3 by the thick curve as a function of the "true" v_2. The gray area is the uncertainty, $\in[0,1]$, determined by the $\pm1\sigma$ statistical uncertainty in the $\Delta\gamma$ measurements. The vertical lines indicate the various measured v_2 values. At present the data precision does not allow a meaningful constraint on $f_{\rm CME}^{\rm EP}$; the limitation comes from the $\Delta\gamma\{\psi_1\}$ measurement, which has an order-of-magnitude larger statistical uncertainty than that of $\Delta\gamma\{\psi_2\}$. With a ten-fold increase in statistics, the constraint would be the dashed curves. This is clearly where the future experimental emphasis should be placed: larger AuAu data samples are being analyzed and more AuAu statistics are to be accumulated; a ZDC upgrade is ongoing in the CMS experiment at the LHC; fixed target experiments at the SPS may be another viable venue where all spectator nucleons are measured in the ZDC possibly allowing a better determination of ψ_1.

4 Summary

In summary, elliptic flow (v_2) develops in relativistic heavy ion collisions from the anisotropic overlap geometry of the participant nucleons. The participant plane azimuthal angle ($\psi_{\rm PP}$), due to fluctuations, does not necessarily coincide with the reaction plane's ($\psi_{\rm RP}$). v_2 with respect to $\psi_{\rm PP}$ is stronger than that with respect to $\psi_{\rm RP}$. This has been known for over a decade. The magnetic field (B) is, on the other hand, produced mainly by spectator protons and its direction fluctuates nominally about $\psi_{\rm RP}$, not $\psi_{\rm PP}$. Therefore, B with respect to $\psi_{\rm PP}$ is weaker than B with respect to $\psi_{\rm RP}$. This has so far not been well appreciated. We have verified these with MC Glauber (MCG) calculations and A Multi-Phase Transport (AMPT) model simulations of AuAu, CuCu, RuRu, ZrZr, and PbPb collisions. One can effectively "change" B in a single nucleus-nucleus collision and, at the same time, "change" v_2 in the opposite direction; the change is significant, as large as 20% in each direction in AuAu collisions. We demonstrate that this opposite behavior in a single collision system, thus with small systematic uncertainties, can be exploited to effectively disentangle the possible chiral magnetic effect (CME) from the v_2-induced background in three-point correlator ($\Delta\gamma$) measurements. We argue that the comparative measurement of $\Delta\gamma$ with respect to $\psi_{\rm RP}$ and $\psi_{\rm PP}$ in the same collision system is superior to isobaric collisions where large systematics persist.

We have applied this novel idea to experimental data; however, due to the poor statistical precision of the data, no conclusion can presently be drawn regarding the possible magnitude of the CME. This calls for future efforts to accumulate data statistics and to improve the capabilities of zero-degree calorimeters. With improved statistics, the novel method we report here should be able to decisively answer the question of the CME in quantum chromodynamics.

References

1 T. Lee and G. Wick, Phys. Rev. D, **9**: 2291 (1974)
2 P. D. Morley and I. A. Schmidt, Z. Phys. C, **26**: 627 (1985)
3 D. Kharzeev, R. Pisarski, and M. H. Tytgat, Phys. Rev. Lett., **81**: 512 (1998), hep-ph/9804221
4 D. Kharzeev and R. D. Pisarski, Phys. Rev. D, **61**: 111901 (2000), hep-ph/9906401
5 D. E. Kharzeev, L. D. McLerran, and H. J. Warringa, Nucl. Phys. A, **803**: 227 (2008), [arXiv:0711.0950[hep-ph]]
6 M. Dine and A. Kusenko, Rev. Mod. Phys., **76**: 1 (2003), URL https://link.aps.org/doi/10.1103/RevModPhys.76.1
7 K. Fukushima, D. E. Kharzeev, and H. J. Warringa, Phys. Rev. D, **78**: 074033 (2008), [arXiv:0808.3382[hep-ph]]
8 D. E. Kharzeev, J. Liao, S. A. Voloshin, and G. Wang, Prog. Part. Nucl. Phys., **88**: 1 (2016), [arXiv:1511.04050[hep-ph]]
9 Q. Li, D. E. Kharzeev, C. Zhang, Y. Huang, I. Pletikosic, A. V. Fedorov, R. D. Zhong, J. A. Schneeloch, G. D. Gu, and T. Valla, Nature Phys., **12**: 550 (2016), [arXiv:1412.6543[cond-mat.str-el]]
10 B. Q. Lv et al, Phys. Rev., **X5**: 031013 (2015), [arXiv:1502.04684[cond-mat.mtrl-sci]]
11 X. Huang et al, Phys. Rev., **X5**: 031023 (2015), [arXiv:1503.01304[cond-mat.mtrl-sci]]
12 I. Arsene et al, (BRAHMS Collaboration), Nucl. Phys. A, **757**: 1 (2005), nucl-ex/0410020
13 K. Adcox et al, (PHENIX Collaboration), Nucl. Phys. A, **757**: 184 (2005), nucl-ex/0410003
14 B. Back et al, (PHOBOS Collaboration), Nucl. Phys. A, **757**: 28 (2005), nucl-ex/0410022
15 J. Adams et al, (STAR Collaboration), Nucl. Phys. A, **757**: 102 (2005), nucl-ex/0501009
16 B. Muller, J. Schukraft, and B. Wyslouch, Ann. Rev. Nucl. Part. Sci., **62**: 361 (2012), [arXiv:1202.3233[hep-ex]]
17 S. A. Voloshin, Phys. Rev. C, **70**: 057901 (2004), hep-ph/0406311
18 W. Reisdorf, and H. Ritter, Ann. Rev. Nucl. Part. Sci., **47**: 663 (1997)
19 J.-Y. Ollitrault, Phys. Rev. D, **46**: 229 (1992)
20 F. Wang, Phys. Rev. C, **81**: 064902 (2010), [arXiv:0911.1482[nucl-ex]]
21 A. Bzdak, V. Koch, and J. Liao, Phys. Rev. C, **81**: 031901 (2010), [arXiv:0912.5050[nucl-th]]
22 S. Schlichting and S. Pratt, Phys. Rev. C, **83**: 014913 (2011), [arXiv:1009.4283[nucl-th]]
23 F. Wang and J. Zhao, Phys. Rev. C, **95**: 051901 (2017), [arXiv:1608.06610[nucl-th]]
24 J. Zhao, Int. J. Mod. Phys. A, **33**: 1830010 (2018), [arXiv:1805.02814[nucl-ex]]
25 B. Abelev et al. (STAR Collaboration), Phys. Rev. Lett., **103**: 251601 (2009), [arXiv:0909.1739[nucl-ex]]
26 B. Abelev et al (STAR Collaboration), Phys. Rev. C, **81**: 054908 (2010), [arXiv:0909.1717[nucl-ex]]
27 B. Abelev et al (ALICE), Phys. Rev. Lett., **110**: 012301 (2013), [arXiv:1207.0900[nucl-ex]]
28 L. Adamczyk et al (STAR), Phys. Rev. C, **88**: 064911 (2013), [arXiv:1302.3802[nucl-ex]]
29 L. Adamczyk et al (STAR), Phys. Rev. Lett. **113**: 052302

(2014), [arXiv:1404.1433[nucl-ex]]
30 L. Adamczyk et al (STAR), Phys. Rev. C, **89**: 044908 (2014), [arXiv:1303.0901[nucl-ex]]
31 V. Khachatryan et al (CMS), Phys. Rev. Lett., **118**: 122301 (2017), [arXiv:1610.00263[nucl-ex]]
32 A. M. Sirunyan et al (CMS), (2017), [arXiv:1708.01602[nucl-ex]]
33 S. Acharya et al (ALICE) (2017), [arXiv:1709.04723[nucl-ex]]
34 J. Zhao (STAR), EPJ Web Conf., **172**: 01005 (2018), [arXiv:1712.00394[hep-ex]]
35 J. Zhao, H. Li, and F. Wang (2017), [arXiv:1705.05410[nucl-ex]]
36 N. Ajitanand, R. A. Lacey, A. Taranenko, and J. Alexander, Phys. Rev. C, **83**: 011901 (2011), [arXiv:1009.5624[nucl-ex]]
37 N. Magdy, S. Shi, J. Liao, N. Ajitanand, and R. A. Lacey (2017), [arXiv:1710.01717[physics.data-an]]
38 S. A. Voloshin, Phys. Rev. Lett., **105**: 172301 (2010), [arXiv:1006.1020[nucl-th]]
39 W.-T. Deng, X.-G. Huang, G.-L. Ma, and G. Wang, Phys. Rev. C, **94**: 041901 (2016), [arXiv:1607.04697[nucl-th]]
40 H.-j. Xu, X. Wang, H. Li, J. Zhao, Z.-W. Lin, C. Shen, and F. Wang, Phys. Rev. Lett., **121**: 022301 (2018), [arXiv:1710.03086[nucl-th]]
41 B. Alver et al (PHOBOS), Phys. Rev. Lett., **98**: 242302 (2007), nucl-ex/0610037
42 M. L. Miller, K. Reygers, S. J. Sanders, and P. Steinberg, Ann. Rev. Nucl. Part. Sci., **57**: 205 (2007), nucl-ex/0701025
43 B. Alver, B. Back, M. Baker, M. Ballintijn, D. Barton et al, Phys. Rev. C, **77**: 014906 (2008), [arXiv:0711.3724[nucl-ex]]
44 X. Zhu, Y. Zhou, H. Xu, and H. Song, Phys. Rev. C, **95**: 044902 (2017), [arXiv:1608.05305[nucl-th]]
45 A. Bzdak and V. Skokov, Phys. Lett. B, **710**: 171 (2012), [arXiv:1111.1949[hep-ph]]
46 W.-T. Deng and X.-G. Huang, Phys. Rev. C, **85**: 044907 (2012), [arXiv:1201.5108[nucl-th]]
47 J. Bloczynski, X.-G. Huang, X. Zhang, and J. Liao, Phys. Lett. B, **718**: 1529 (2013), 1209.6594; Nucl. Phys. A, **939**: 85 (2015), [arXiv:1311.5451[nucl-th]]
48 H.-j. Xu, L. Pang, and Q. Wang, Phys. Rev. C, **89**: 064902 (2014), [arXiv:1404.2663[hep-ph]]
49 M. Rybczynski and W. Broniowski, Phys. Rev. C, **84**: 064913 (2011), [arXiv:1110.2609[nucl-th]]
50 M. Bender, P.-H. Heenen, and P.-G. Reinhard, Rev. Mod. Phys., **75**: 121 (2003)
51 J. Erler, N. Birge, M. Kortelainen, W. Nazarewicz, E. Olsen, A. M. Perhac, and M. Stoitsov, Nature, **486**: 509 (2012)
52 E. Chabanat, P. Bonche, P. Haensel, J. Meyer, and R. Schaeffer, Nucl. Phys. A, **635**: 231 (1998); Nucl. Phys. A, **643**: 441 (1998)
53 J. Bartel, P. Quentin, M. Brack, C. Guet, and H. B. Hakansson, Nucl. Phys. A, **386**: 79 (1982)
54 P. Ring and P. Schuck, *The Nuclear Many-body Problem*, Texts and monographs in physics (Springer, 2000), URL https://books.google.com/books?id=QmQ4nQEACAAJ
55 X. B. Wang, J. L. Friar, and A. C. Hayes, Phys. Rev. C, **94**: 034314 (2016), [arXiv:1607.02149[nucl-th]]
56 A. M. Poskanzer and S. Voloshin, Phys. Rev. C, **58**: 1671 (1998), nucl-ex/9805001
57 B. Abelev et al (ALICE), Phys. Rev. Lett., **111**: 232302 (2013), [arXiv:1306.4145[nucl-ex]]
58 L. Adamczyk et al (STAR), Phys. Rev. Lett., **118**, 012301 (2017), [arXiv:1608.04100[nucl-ex]]
59 B. Abelev et al (STAR Collaboration), Phys. Rev. C, **79**: 034909 (2009), [arXiv:0808.2041[nucl-ex]]
60 Z.-W. Lin and C. Ko, Phys. Rev. C, **65**: 034904 (2002), nucl-th/0108039
61 Z.-W. Lin, C. M. Ko, B.-A. Li, B. Zhang, and S. Pal, Phys. Rev. C, **72**: 064901 (2005), nucl-th/0411110
62 Z.-W. Lin, Phys. Rev. C, **90**: 014904 (2014), [arXiv:1403.6321[nucl-th]]
63 G.-L. Ma and B. Zhang, Phys. Lett. B, **700**: 39 (2011), [arXiv:1101.1701[nucl-th]]
64 G.-L. Ma and Z.-W. Lin, Phys. Rev. C, **93**, 054911 (2016), [arXiv:1601.08160[nucl-th]]
65 L. He, T. Edmonds, Z.-W. Lin, F. Liu, D. Molnar, and F. Wang, Phys. Lett. B, **753**: 506 (2016), [arXiv:1502.05572[nucl-th]]
66 H. Li, L. He, Z.-W. Lin, D. Molnar, F. Wang, and W. Xie, Phys. Rev. C, **93**: 051901 (2016), [arXiv:1601.05390[nucl-th]]
67 H. Li, L. He, Z.-W. Lin, D. Molnar, F. Wang, and W. Xie, Phys. Rev. C, **96**: 014901 (2017), [arXiv:1604.07387[nucl-th]]
68 H.-j. Xu, Z. Li, and H. Song, Phys. Rev. C, **93**: 064905 (2016), [arXiv:1602.02029[nucl-th]]
69 U. Heinz and R. Snellings, Ann. Rev. Nucl. Part. Sci., **63**: 123 (2013), [arXiv:1301.2826[nucl-th]]
70 G. Wang (STAR), Nucl. Phys. A, **774**, 515 (2006), nucl-ex/0510034
71 S. A. Voloshin (STAR), J. Phys. G, **34**: S883 (2007), nucl-ex/0701038
72 J. Adams et al (STAR Collaboration), Phys. Rev. C, **72**: 014904 (2005), nucl-ex/0409033
73 N. M. Abdelwahab et al (STAR), Phys. Lett. B, **745**: 40 (2015), [arXiv:1409.2043[nucl-ex]]